INTERNATIONAL JOURNAL OFAUTOMOTIVE AND MECHANICAL ENGINEERING (IJAME)
ISSN: 2229-8649 e-ISSN: 2180-1606
VOL. 18, ISSUE 3, 8959 –8977
DOI: https://doi.org/10.15282/ijame.18.3.2021.09.0686

ORIGINAL ARTICLE

Fabrication and Modelling of Tribological Performance of Al-Si/12Al_2O_3/2MoS_2 Composite using Taguchi Technique

H.K. Vuddagiri[1]*, Srinivas Vadapalli[2], Jaikumar Sagari[2] and R. Sivasankara Raju[3]

[1]Department of Mechanical Engineering, Avanthi Institute of Engineering and Technology,531113 Narsipatnam, India.
[2]Department of Mechanical Engineering, GITAM deemed to be University, 530045 Visakhapatnam, Andhra Pradesh, India.
[3]Department of Mechanical Engineering, Aditya Institute of Technology and Management, 532201 Tekkali, India.

ABSTRACT – This paper investigates the effect of mechanical, microstructural and dry sliding wear behaviour of Al-Si/2wt%MoS_2, Al-Si/12wt%Al_2O_3, and Al-Si/12wt% Al_2O_3/2wt%MoS_2 composites that prepared using the stir-casting route. To avoid friction and wear at the interfaces of materials, an attempt has been made by adding solid lubricant MoS2 to build such a self-lubricating composite with Al-matrix. The tribological analysis has been described based on the Taguchi orthogonal array (L27). Three variables combination such as sliding velocity, sliding distance and contact pressure are used for this study to determine the tribological responses, i.e. wear rate and coefficient of friction. The properties of composites were improved by increasing the weight % of MoS_2 and Al_2O_3. The tensile strength of Al-Si/2MoS_2, Al-Si/12Al_2O_3, and Al-Si/12 Al_2O_3/2MoS_2 composites is 6.02%, 12.46%, and 2.44% compared to the base matrix. The addition of MoS_2 helps the hybrid composite to attain better tribological properties with a slightly lower specific strength. Analysis of variance showed that the composites such as Al-Si/2 MoS_2 and Al-Si/12Al_2O_3/2MoS_2 were strongly influenced by the pressure in wear rate. Similarly, sliding velocity affects the coefficient of friction for Al-Si/2MoS_2. Wear tracks formed during the dry slide process were analysed using optical and SEM with an EDS. It was discovered that pressure plays a vital effect in the wear mechanism. The hybrid composite (Al-Si/12 Al_2O_3/2MoS_2) material can be utilised in place of conventional materials in tribological demanding automotive applications.

ARTICLE HISTORY
Received:2nd April 2021
Revised:19th July 2021
Accepted: 25th Aug 2021

KEYWORDS
AMCs;
MoS_2;
Al_2O_3;
Wear rate;
Coefficient of friction

INTRODUCTION

In recent times, technologists constantly develop novel materials, having lightweight and good reliability parts, much like in the vehicle sector, to meet the ever-increasing demands and complexity of the new technologies. It is difficult to obtain all of those previously established qualities using traditional materials. A number of economic benefits have been associated with aluminium matrix composites, being good modulus of elasticity, wear resistance, low cost, high strength, and thermal conductivity, along with use in aircraft, space, defence, and automobiles [1–3].

Mostly when talking about wear resistance, lubrication is important to mitigate. That is usually difficult to do but can be done while interfaces are wearing components. Self-lubricated components purged completely during wear. Graphite and MoS_2 are common lubricants for high load and temperature. Few lubricants do not need a liquid medium to have low friction. While they are in the solid state to decomposition at high temperature, it is difficult to stay the liquid lubricant for some time, and then solid lubricants are used to meet the specific requirements[4–8].

The MoS_2 has a number of other noteworthy properties, such as lubricity at high loads, fret safety, anti-slip effect, wear resistance, and anti-corrosion. Lubricant particle size has an effect on friction. The larger particles work well at slow speeds, while the finer particles are best on rougher surfaces. These particles may be used to improve their properties also in liquid lubricants[9–12]. More related compounds include polytetrafluoroethylene (PTU), calcium fluoride (CaF), and cerium tungsten disulfide (CeW12), have the same effect [13]. The interface of MoS_2 appears to be linear with lamella directed in the direction of motion, serving as a pathway for relative motion but hindering interaction through different sliding components under varying strain [14]. Using lubricants is useful to keep materials from adhering to each other, due to a weak bond with the surface. These layers glide proportionally with a minimal force and thus achieve low drag characteristics. For this function, MoS_2 has been utilized in industrial conditions.

The mechanical and tribologically efficient preparation of Al/MOS_2 (3 and 10% wt) composites using a hot press process has been researched by Chen and others [8]. Results show that the hardness and compression strength of 3% MoS_2 composite is somewhat higher than that of 0% MoS_2 composite, while the strength of composites with 10% MoS_2 content was dramatically reduced. The wear rate of the composite with 10% MoS_2 increased rapidly at 50 N load and 0.69 m/s sliding speed, while the composites at 30 N load and 0.69 m/s sliding speed had low and stable wear rates, with MML present shape across the wear track. Rajesh et al. [6] studied on AA2219/xMoS_2 (x = 1.5, 3 and 4.5) composites, which were subjected to lubricated wear with tyreoil. The study was analysed using a 2D plot and analysis of variance (ANOVA). In this analysis, the process variables such as load, velocity, %MoS_2 and hardness of disc were considered.

*CORRESPONDING AUTHOR | Hari Kiran Vuddagiri | ✉ harikiran3285@gmail.com

The author concluded from these findings that the wear rate increases proportionally with applied force and disc hardness but reduced with the weight % of MoS_2.

Harpreet et al. [13] studied the tribological effect of composites during lubrication environments such as MoS_2 molybdenum disulphide, boric acid (H3BO3) and multi-concentrational carbon nanotubes (MWCNT) in paraffin SN500 oiled. The composites were Al-SiC, Al-B_4C and Al-SiC-B_4C. In contrast to MoS_2, which exhibits moderate frictional improvement in performance, the compounds H3BO3 and MWCNT exhibit significant friction and wear improvement. Kanthavel et al.[15] examined the tribological properties of Al/5% Al_2O_3/ (5-10%) MoS_2 composites produced by powder metallurgy. At constant sliding speeds of 0.5 m/s and distances of 1000 m, Al/5% Al_2O_3/5% MoS_2 exhibits the least amount of wear and coefficient of friction. The study shows that adding 10% MoS_2 to the composite may not enhance tribological properties. Moharami [16] investigated the influence of the interdependence among the sliding distance and the wear rate on the dry sliding wear behaviour of as-cast (Al-30Mg2Si) and friction stir process (FSP) samples at ambient and elevated temperatures. The author demonstrated that FSP-induced microstructural change significantly increased the wear resistance of an Al-30Mg_2Si alloy at ambient conditions. Decreased wear rate (at 1000 m) and average COF (compared to as-cast) were also achieved by increasing pass number. This was caused by small Mg2Si particles in the FSP substratum which likely hindered the development of grain at a higher temperature and transformed the serious adhesive mechanisms.

Ali [17] investigated the influence of several tool pin topologies on the combining capability of AA6061-T6 and Al-20%Mg_2Si with FSW. This study was conducted using a flow rate of 80 mm/min and a rotation speed of 1000 rpm. They demonstrated that the triangle tapered (TT) tool reduced the average grain size of the AA6061 alloy from 18.4 mm to 4.6 mm and the Mg_2Si particles from 115 mm to 7.5 mm, due to intense dynamic recrystallisation and particle-induced pinning effects. Low solubility in alloys of AA6061-T6 and Al-Mg2Si is thought to have aided the development of Fe rich intermetallic compounds. Frictions of the joints AA6061/Al-Mg_2Si is greatly reduced within the TT joints because of the steady increase of the hard Mg_2Si particles in the nuggets [18]. The average diameters of the naturally existing Mg_2Si phase also influenced the corrosion attack on the AA6061/Al-Mg_2Si junction. The sample made with a TT tool had the least corrosion attack in NaCl solution due to the finer average Mg_2Si phase diameters and shorter interparticle (Mg_2Si) distances. They determined that a triangular pin tool is recommended for the different Al/composite welding because of the favourable flow of material, diffusion, and fragmentation caused by the tool. Vinoth et al. [19] studied the impact of Al-Si-10Mg, Al-Si-10Mg/MoS_2 composites in mechanical and tribological aspects. They found that adding MoS_2 particles reduced composite properties but improved wear resistance. The $2MoS_2$ and $4MoS_2$ composites demonstrate a reduced wear rate by 46% and 62%, respectively, compared to the basic alloy.

Patle and colleagues used friction stir processing (FSP) to make an AA7075-B4C/MoS2 hybrid composite [20]. Typically, a 12-h heat treatment solution treatment at room temperature of 50 °C, followed by artificial quenching and 0.5-h solution treatment time, which are both conducted for an additional 24-h duration, will result in soft leather hardening desired. The composites hardness improved from 156 to 160HV. The B_4C and MoS2 seem to diminish the direct interdependence between the counter and pin. To check the stability of Al2219/n%B_4C and Al/n%B_4C/2%MoS_2 nanocomposites, Siddesh [21] prepared the samples and checked them at high temperature using a pin-disc wear test rig. The glazing layers and oxide film on the slide pins visibly speed up their wear rate according to Al2219/n%B_4C composites. Also, during metal-to-sliding phase, these layers serve as a barrier between the surfaces. At lower temperatures, they observed plastic deformation and delamination in Al2219, but at higher temperatures of 100 °C, they observed oxide layer rupture and slightly extended grooves of the glazing layer. Jeyasimman et al.[22] explained that the sliding wear for given load increases as the amount of sliding distance and the speed of sliding increases. According to the paper, with the addition of nanoparticles Al_2O_3 (30-60 nm) and TiCp (200 nm) the composite exhibited less wear resistance. The author compared mono reinforced particulates of TiC and Al_2O_3 in the AA6061 alloy with the hybrid. The hybrid nanocomposite (AA6061/TiC/Al_2O_3) displayed a greater wear resistance.

According to the aforementioned literature, it was determined that the mechanical and tribological properties of Al-Si alloys reinforced by Al_2O_3 and MoS_2 were still not completely examined. As a result, an attempt was undertaken to synthesize a hybrid Al-Si/Al_2O_3/MoS_2 composite in producing superior mechanical and dry wear resistance qualities. Taguchi OA has been adopted to determine the wear behaviour of composite materials during dry sliding in order to determine the optimal wear setting.

METHODOLOGY

Composites Fabrication using Stir Casting Route

In this study, the stir casting route was adopted for the fabrication of composites. The matrix in Table 1 was chopped into pieces and filled in a graphite crucible, and melted in a bottom-pouring furnace (Model: ENV120T, Naskar) beyond its thermal stability of 750 °C. The crucible holds the melted aluminium. On the other side, in order to cleanse and remove the artificial hydrox coating and adsorbed gases on the Al_2O_3 and MoS_2 particles, they were preheated in a hot oven for 2 hours at 600 °C. The melting permitted to cool in between its liquid and solids stages but also kept in a halved form. If the metal is totally melted and the temperature is placed well above the liquid, the melting rate is halved. To improve wettability, magnesium ribbon is incorporated into the molten metal prior to reinforcement. The estimated reinforcement volume is applied to molten metal 3-4 times rather than only added at once in the whirlpool. The mixture was stirred for 10 minutes and refined into a liquid form with a furnace apprehended at 750 ± 5°C. After the process, the melt is poured

into the preheated mild steel mould. All the composites (i.e., Al-Si/2wt%MoS_2, Al-Si/12wt%Al_2O_3, and Al-Si/12wt%Al_2O_3/2wt%MoS_2) adopted the same methodology in preparation.

Table 1. Elemental composition of Al-Si matrix.

Element	Si	Fe	Cr	Cu	Mn	Zn	Mg	Remain
Content (%)	0.80 - 1.2	0.50 - 0.80	≤ 0.20	≤ 0.10	≤ 0.050	≤ 0.050	≤ 0.010	Al

Materials Testing and Methods

The fundamental objective of this work is to establish to characterize the feasibility of wear-resistant and the friction properties of developed hybrid matrix composites materials. In this study, the AMCs are prepared using MoS_2 and Al_2O_3 as reinforcements. The MoS_2 particulates was supplied by Intelligent Materials Private Limited, Punjab and Al_2O_3 particulates are obtained from Sajan overseas private limited, Ahmadabad. The particulate size of MoS_2 and Al_2O_3 having average size of 45 µm. The shape of the reinforced materials is shown in Figure 1.

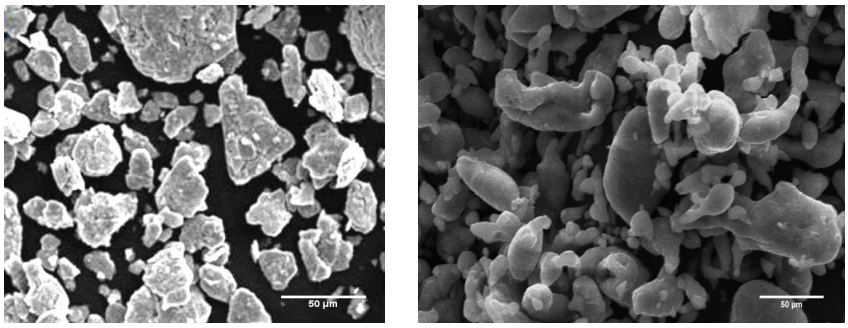

(a) (b)

Figure 1. Reinforced particulates: (a) MoS_2 (b) Al_2O_3.

Hardness testing (Model: MRB HM-RB/187), tensile strength testing (Model: ETM-ER3), metallurgical analysis for surface by ASTM E-7-17, adopting SEM (Model: JEOL JSM-5600LV)), density measurement, and pin-on-disc wear tester (Model: TE-165-SPOD) are among the characterisation methods used. The Archimedes theory was taken to calculate the densities of a stir cast hybrid reinforced AMCs, which provides an accurate and quicker process to determine the density of certain irregular solid particles. The metals structure was examined at different scales using an optical microscope (Model: METZ-797) to provide descriptive and analytical characterization. The form, scale, and scattering of structure oxide fillers were investigated using a metallurgical microscope in this study. The samples were polished with fine grit and then swabbed with a Keller test solution for 20-40 seconds to study the structure of composites.

According to the ASTM G99-95a standard, a pin-on-disc tester (Model: TE-165-SPOD) was used to determine the tribological performances, and the test was performed at room temperature [23]. The counter disc is made of steel material that has approximately 62 HRC (EN-31A) hardness. The disc had a diameter of up to 80 mm with a thickness of 8 mm. The dimension of the pin sample is 35 mm long and 8 mm in diameter. The pin specimens are polished with fine sandpaper in grades 600 to 1200 prior to carrying out the tribological test. The pin and disc were cleaned with acetone before and after wear. The wear rate determines the quantity of wear loss/volume loss or linear dimension change per unit of normal force per sliding distance applied—the wear rate measured in mm^3/m [2,24]. The COF of the specimens has been recorded automatically throughout the test. Further, all investigations were repeated three times with the average values stated in each situation to confirm the reliability of the results.

Experimental Design with Taguchi Approach (L27)

Doing a single experiment is too difficult with precise factorial design as doing a single experiment with more control factors. The Taguchi procedure provides a well-designed orthogonal structure to overcome the issue and helps to test the whole parameter with the exception of minimal experiments. Taguchi's method is an interpretive paradigm to learn about the performance of a process. ANOVA was used to evaluate the results [25–27]. ANOVA is a method for determining the most important factor and quantifying the variation into distinguishable causes of deviation. The F- test is a reference deviation factor. If variance analysis was performed on a set of statistics, the adjusted square sums were assigned to the quality factors. By comparing this value to the total sum of squares, the percentage of contribution in each variable can be determined. P-value (meaning probability) is determined by the meaning of F. The P-value is a variable typically ≤ 0.05 (with 95% confidence); therefore, the presence of data-point interactions is significant.

In this study, three variables are used at three levels. The variables applied were pressure (P), sliding distance (SD) and sliding velocity (SV), which were employed to measure tribological quantities, i.e. wear rate (WR) and coefficient of friction(CF). The chosen variables are shown in Table 2, while Table 3 shows the 27 tests that make up the evaluation plan. The variables are reserved in a column of one, two, and five; the other columns specified in interactions, under the assumption that flexibility degree would be essentially equivalent to a number of certain response variables upon factor analysis. The overall degree of freedom required for the overall experiment is related to the number of factors, levels, and

associated interactions. The tribological quantities and their signal to noise (SN) values of cast materials are shown in Table 4 and Table 5.

Table 2. Variables with selection levels.

Variables	Units/ Levels	Level 1	Level 2	Level 3
Sliding Velocity (SV)	m/s	1	1.5	2
Sliding Distance (SD)	m	600	900	1200
Pressure (P)	Kg-f /cm^2	2.04	3.06	4.08

Table 3. Experimental layout of Taguchi orthogonal array (L27).

Run	SV	SD	P	Run	SV	SD	P
1	1	600	2.04	15	1.5	900	4.08
2	1	600	3.06	16	1.5	1200	2.04
3	1	600	4.08	17	1.5	1200	3.06
4	1	900	2.04	18	1.5	1200	4.08
5	1	900	3.06	19	2	600	2.04
6	1	900	4.08	20	2	600	3.06
7	1	1200	2.04	21	2	600	4.08
8	1	1200	3.06	22	2	900	2.04
9	1	1200	4.08	23	2	900	3.06
10	1.5	600	2.04	24	2	900	4.08
11	1.5	600	3.06	25	2	1200	2.04
12	1.5	600	4.08	26	2	1200	3.06
13	1.5	900	2.04	27	2	1200	4.08
14	1.5	900	3.06				

Table 4. Responses of WR of composites with SN ratios.

Run	Al-Si		Al-Si/2MoS_2		Al-Si/12Al_2O_3		Al-Si /1212Al_2O_3/2MoS_2	
	WR	SNRA	WR	SNRA	WR	SNRA	WR	SNRA
1	2.383	-7.542	1.940	-5.757	1.787	-5.044	1.039	-0.329
2	2.678	-8.558	2.161	-6.693	2.033	-6.162	1.259	-2.003
3	2.974	-9.467	2.382	-7.538	2.279	-7.153	1.480	-3.406
4	2.461	-7.822	1.980	-5.931	1.795	-5.081	1.078	-0.652
5	2.725	-8.707	2.200	-6.850	2.059	-6.273	1.299	-2.270
6	2.989	-9.511	2.421	-7.680	2.323	-7.321	1.519	-3.634
7	2.422	-7.683	2.019	-6.102	1.791	-5.063	1.117	-0.964
8	2.702	-8.633	2.240	-7.003	2.046	-6.218	1.338	-2.530
9	2.981	-9.489	2.460	-7.820	2.301	-7.238	1.559	-3.856
10	2.054	-6.254	1.735	-4.785	1.541	-3.755	0.833	1.584
11	2.350	-7.421	1.956	-5.825	1.786	-5.040	1.054	-0.457
12	2.645	-8.450	2.176	-6.754	2.032	-6.159	1.275	-2.109
13	2.028	-6.141	1.774	-4.980	1.362	-2.684	0.873	1.183
14	2.272	-7.128	1.995	-5.998	1.606	-4.115	1.093	-0.775
15	2.516	-8.014	2.216	-6.910	1.850	-5.343	1.314	-2.373
16	2.041	-6.198	1.814	-5.170	1.451	-3.236	0.912	0.800
17	2.311	-7.276	2.034	-6.168	1.696	-4.590	1.133	-1.082
18	2.581	-8.235	2.255	-7.063	1.941	-5.761	1.353	-2.629
19	1.890	-5.530	1.632	-4.255	1.418	-3.031	0.731	2.726
20	2.186	-6.791	1.853	-5.357	1.663	-4.419	0.951	0.433
21	2.481	-7.893	2.074	-6.335	1.909	-5.616	1.172	-1.379
22	1.663	-4.418	1.672	-4.462	0.997	0.026	0.770	2.271
23	1.887	-5.515	1.892	-5.539	1.221	-1.734	0.991	0.081
24	2.111	-6.490	2.113	-6.498	1.445	-3.197	1.211	-1.666
25	1.777	-4.992	1.711	-4.664	1.207	-1.636	0.809	1.838
26	2.036	-6.177	1.932	-5.718	1.442	-3.180	1.030	-0.257
27	2.296	-7.220	2.152	-6.658	1.677	-4.490	1.251	-1.943

Table 5. Responses of CF of composites with SN ratios.

Run	Al-Si		Al-Si/2MoS_2		Al-Si/12Al_2O_3		Al-Si /12Al_2O_3/2MoS_2	
	COF	SNRA	COF	SNRA	COF	SNRA	COF	SNRA
1	0.288	10.806	0.165	15.658	0.148	16.576	0.132	17.604
2	0.296	10.572	0.173	15.252	0.163	15.757	0.153	16.294
3	0.304	10.343	0.181	14.864	0.180	14.915	0.179	14.966
4	0.285	10.895	0.162	15.813	0.156	16.116	0.151	16.431
5	0.293	10.658	0.170	15.400	0.170	15.370	0.171	15.341
6	0.301	10.427	0.178	15.005	0.186	14.593	0.195	14.199
7	0.282	10.984	0.159	15.971	0.163	15.783	0.166	15.599
8	0.290	10.745	0.167	15.550	0.176	15.095	0.185	14.663
9	0.298	10.512	0.175	15.149	0.191	14.370	0.208	13.655
10	0.283	10.962	0.160	15.931	0.145	16.774	0.130	17.707
11	0.291	10.723	0.168	15.513	0.159	15.997	0.149	16.511
12	0.299	10.491	0.176	15.113	0.174	15.188	0.173	15.263
13	0.280	11.052	0.157	16.091	0.151	16.401	0.146	16.723
14	0.288	10.810	0.165	15.665	0.164	15.690	0.164	15.715
15	0.296	10.576	0.173	15.259	0.179	14.938	0.186	14.629
16	0.277	11.143	0.154	16.254	0.156	16.151	0.158	16.050
17	0.285	10.899	0.162	15.820	0.168	15.492	0.174	15.177
18	0.293	10.662	0.170	15.407	0.182	14.787	0.195	14.209
19	0.281	11.040	0.157	16.071	0.150	16.485	0.143	16.919
20	0.288	10.800	0.165	15.646	0.162	15.792	0.160	15.940
21	0.296	10.565	0.173	15.240	0.177	15.055	0.180	14.872
22	0.278	11.131	0.154	16.234	0.155	16.220	0.155	16.205
23	0.286	10.888	0.162	15.801	0.166	15.580	0.171	15.365
24	0.293	10.651	0.170	15.388	0.180	14.891	0.190	14.420
25	0.275	11.223	0.151	16.400	0.157	16.068	0.163	15.749
26	0.283	10.977	0.159	15.958	0.168	15.473	0.178	15.013
27	0.290	10.738	0.167	15.538	0.182	14.822	0.196	14.160

RESULTS AND DISCUSSION

Physical and Mechanical Properties of Cast Composites

The tensile strength (UTS) of Al-Si/2% MoS_2 decreased by 6.41% to Al-Si alloy, as shown in Figure 2(a). Also, the strength of Al-Si/12Al_2O_3 and hybrid composites (Al-Si/2MoS_2/12Al2O3) increased by 11.08% and 2.38%, respectively. The improvement of UTS may be caused to the strong Al_2O_3 reinforcement particles lead to the homogenous dispersion in the materials and acts as a load barrier. The composite Al-Si/12Al_2O_3 exhibited better UTS than other materials. However, the decreased UTS in the hybrid and MoS_2 composites can be attributable to low ultimate MoS_2 (tolerance of 70 MPa) tensile strength compared with the Al-Si matrix (at 162 MPa) resulting in a decrease in UTS of MoS_2 composites. Similarly, the composite elongation in Figure 2(a) revealed that the Al_2O_3 and MoS_2 addition decreased the ductility of the composite slightly than the Al-Si alloy. The addition of 2 wt.% of MOS_2, 12% of Al_2O_3 and 2% of MoS_2 and 12% of Al_2O_3 led to a decline of elongation by 18.67%, 26.51% and 22.59%, which caused to increases the composite hardness.

The Al_2O_3 density (3.95 g/cm^3) is higher than in Al-Si (2.71 g/cm^3), such that the Al_2O_3 volume enhances the composite density, as in the Al-Si matrix. As the particle density of MoS_2 (5.03 g/cm^3) is significantly greater than the Al-Si density, increasing the reinforcing weight fraction (such as Al_2O_3 and MoS_2) could increase the characteristics of the hybrid composites. Figure 2(b) shows that the density of mono (Al-Si/2% MoS_2 and Al-Si/12% Al_2O_3) increased by 1.12% and 1.48%, respectively, compared to Al-Si. Similarly, hybrid composites (Al-Si/2MoS_2/ 12Al_2O_3) have a 2.82% improvement in density compared to Al-Si alloy. With the increased content of MoS_2 and Al_2O_3 reinforcement, the hardness of the composites in Figure 2(b) increased. The potential determinant Al_2O_3 filler particles lead to the homogenous distribution in the matrix, caused to harden the composite. The mono-reinforced (12% Al_2O_3) composites have a higher hardness than the hybrid (Al_2O_3 and MoS_2) composites owing to MoS_2, which is soft in nature and has a lamellar structure. Since the thermal expansion (CTE) of MoS_2 particles (8.43 m/m°C) is lower than Al-Si (22.3 m/m°C), an abundance of dislocations produced at the particle-matrix interface during the solidification, increasing the matrix hardness further.

Metallographic Analysis of Composites

Figure 3 illustrates grain refinement in composites as a result of proper stirring and the use of necessary control performance, which aids in dispersing particles (Al_2O_3, MoS_2) inside the matrix. Figure 3(a) illustrates the microstructure of the Al-Si matrix. The images indicate that the matrix is free of cracks and agglomeration. The morphology of the composites (Al-Si/2MoS_2) is becoming progressively refined. The heterogeneous nucleation induced by the MoS_2 is responsible for this structural refinement. Because of the larger Al_2O_3 quality, the Al-Si/12Al_2O_3 composite has the finest

crystalline structure. The pinning action of dispersoids at grain boundaries caused the hybrid composites in Figure 3(d) to diminish in certain grain borders during solidification. The Orowan Mechanism elucidates the relationship between the fineness of composite grain and strength [28–30].

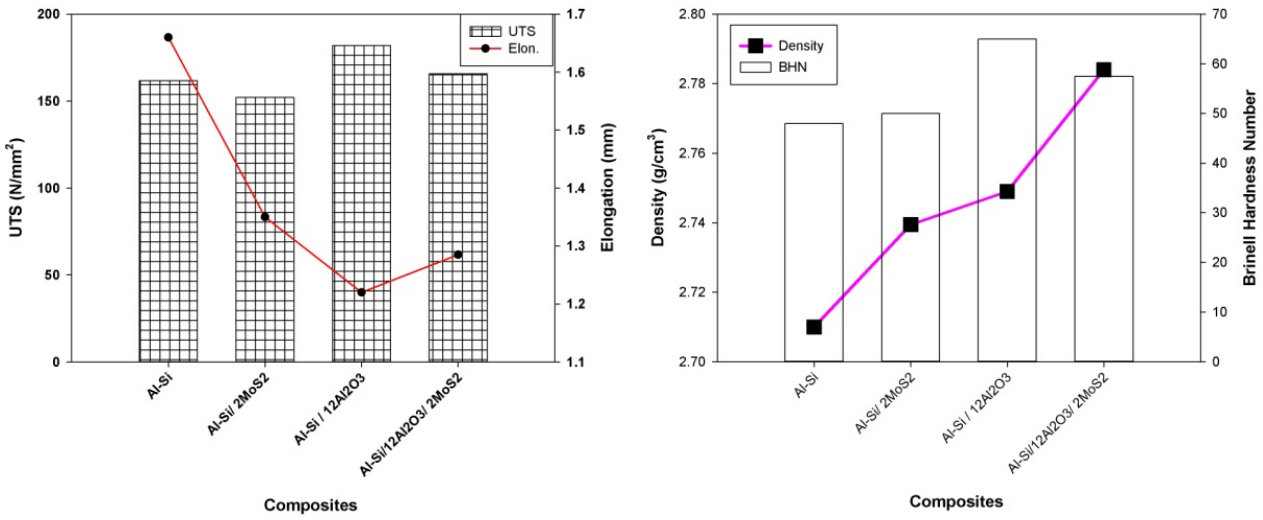

(a) (b)

Figure 2. Properties of composites: (a) UTS and elongation, (b) density and hardness.

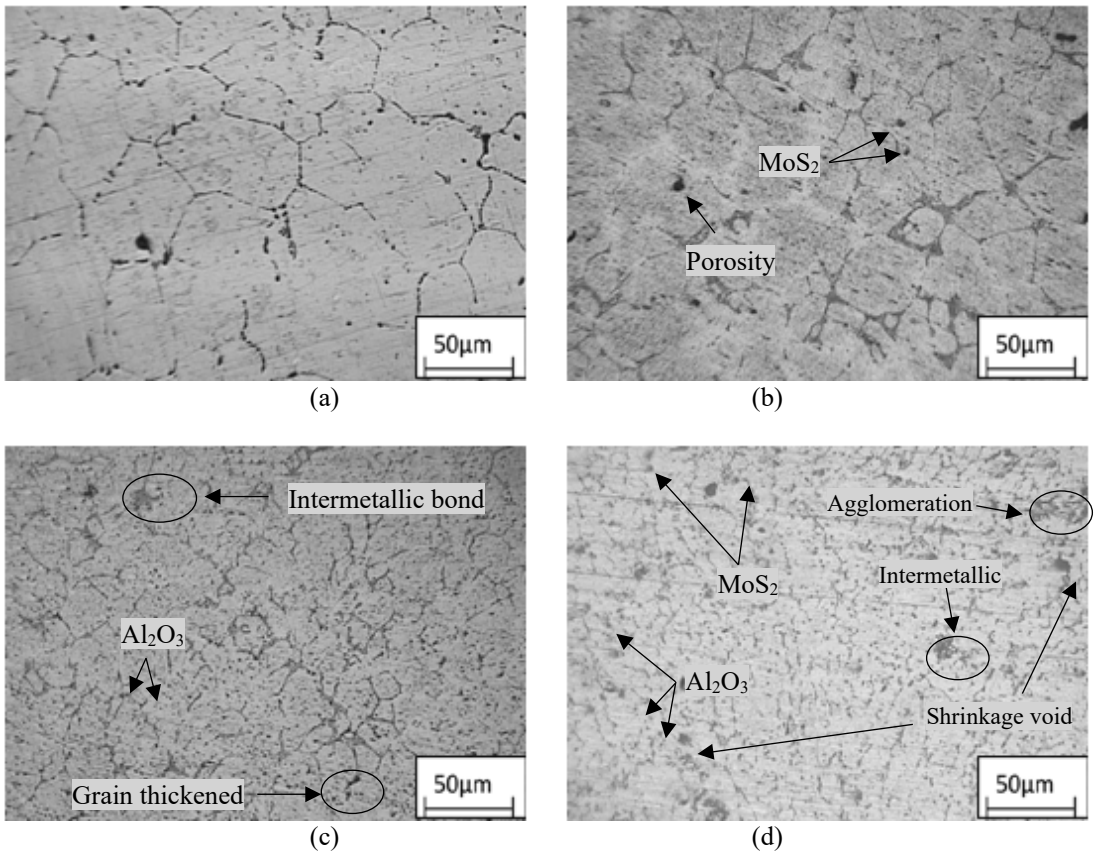

(a) (b)

(c) (d)

Figure 3. Metallographic images of (a) Al-Si (b) Al-Si/2MoS_2 (c) Al-Si -12 Al_2O_3 (d) Al-Si /2MoS_2/12Al_2O_3 composites.

Fine granules increase the strength and toughness of the cast composite because of the increased heterogeneous nucleation rate caused by incoherent particles in the material. Cast composite grains are often significantly finer than Al-Si alloy, see Figure 3(a). The volume per cent was also determined using an image processing analyzer and is shown in Figure 4.

Tribological Examination of Cast Composites using Surface Plots

The main objective of the current work is to found the optimum process parameters to obtain minimum wear rate (WR) and coefficient of friction (CF). The model responses were analysed by plotting 3D-response surface plots. Surface

plots were drawn for a combination of the process variables such as sliding velocity (SV) and sliding distance (SD) for Al-Si and all cast composites such as Al-Si/2MoS_2, Al-Si/ 12Al_2O_3, and Al-Si /12Al_2O_3/ 2MoS_2.

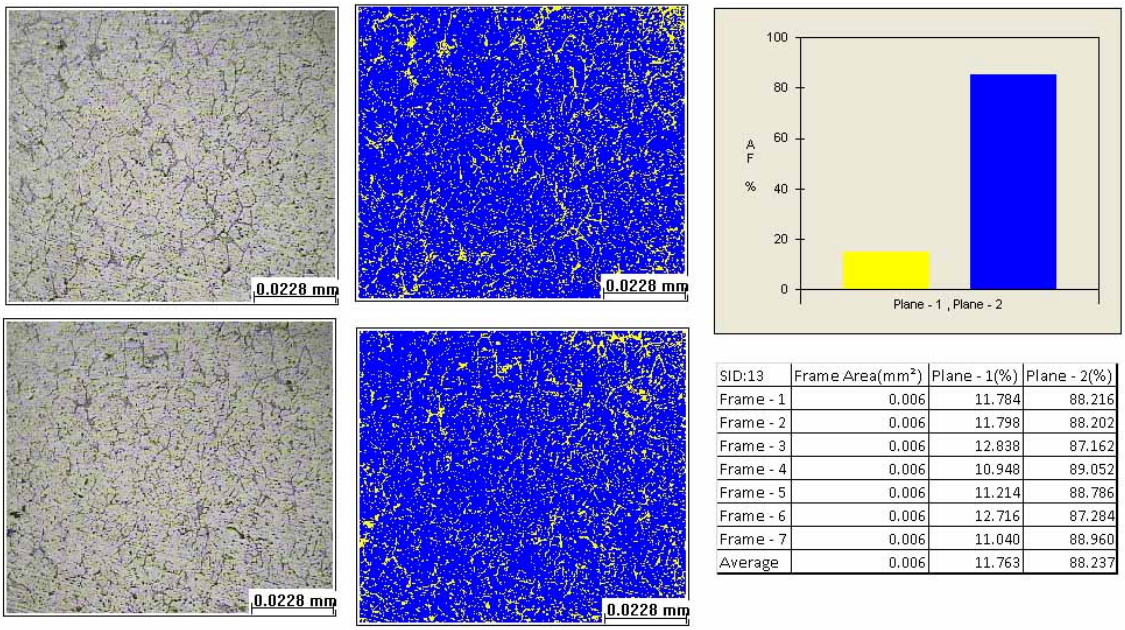

SID:13	Frame Area(mm²)	Plane - 1(%)	Plane - 2(%)
Frame - 1	0.006	11.784	88.216
Frame - 2	0.006	11.798	88.202
Frame - 3	0.006	12.838	87.162
Frame - 4	0.006	10.948	89.052
Frame - 5	0.006	11.214	88.786
Frame - 6	0.006	12.716	87.284
Frame - 7	0.006	11.040	88.960
Average	0.006	11.763	88.237

Figure 4. The volumetric proportion of reinforced particles and their dispersion in Al-Si/ 12Al2O3 composite.

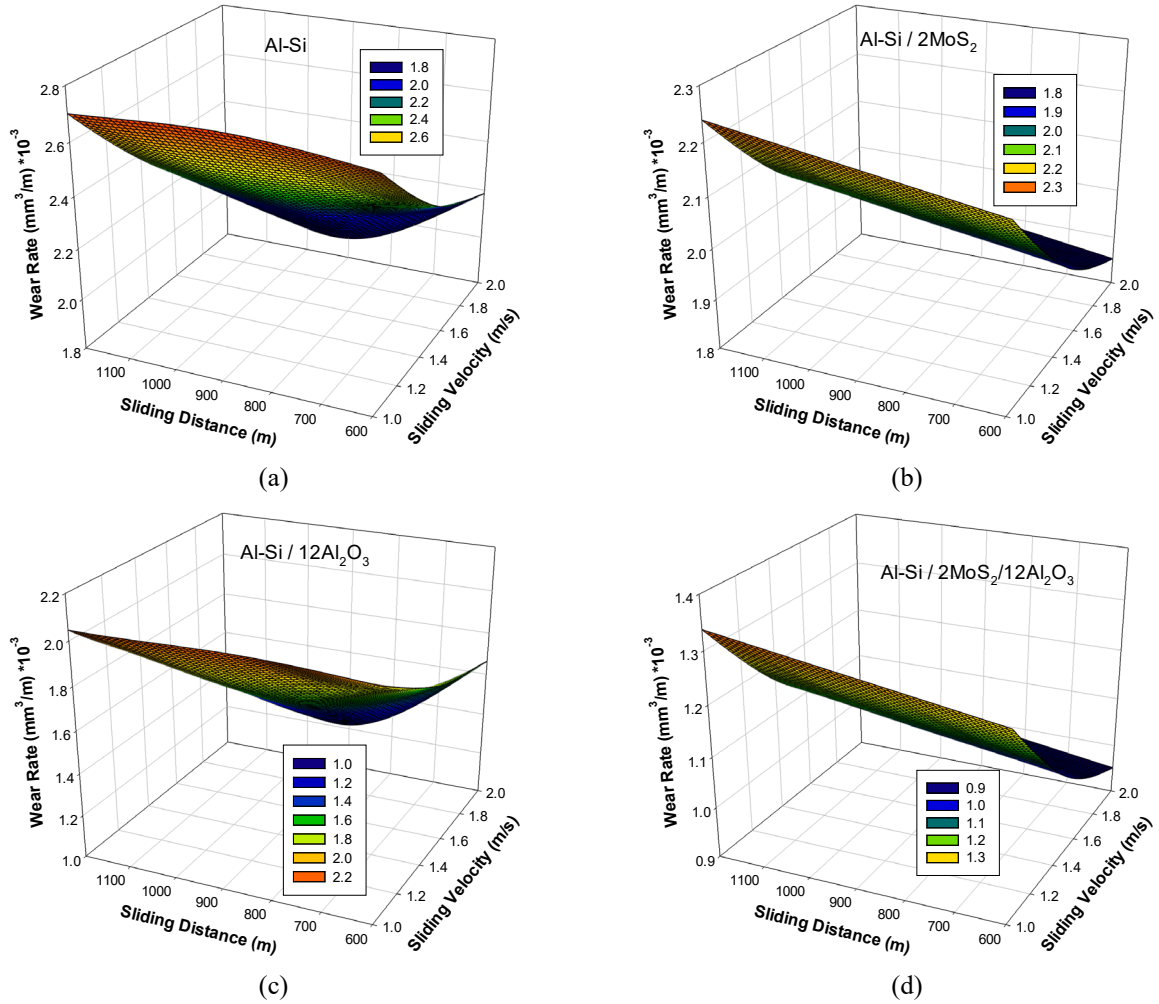

Figure 5. Combined effect of wear rate on composites (a) Al-Si (b) Al-Si /2MoS_2 (c) Al-Si /12Al_2O_3 (d) Al-Si /2MoS_2/ 12Al_2O_3.s

The combined effect on the wear rate of cast materials was carried at a constant pressure of 3.06 kg-f/cm^2 with varying SD and SV, shown in Figure 5(a) to 5(d). Figure 5(a) and 5(c) show that as the sliding distance increases, the wear rate decreases until it exceeds 750 m, after which it rises due to the loss of the intrinsic strength of AMCs and also may be

owing to friction offered by counterface (steel disc). While the sliding distance affects the wear rate, it reduces when coupled with the sliding velocity since the sliding distance dominates the load [31,32]. Hard phase particles (Al_2O_3) are not able to support a matrix against a higher sliding distance; thus, a mildly brittle fracture will occur and causing increase in wear rate.

However, when sliding velocity (SV) increases, the rate of wear decreases. Wear loss decreased slightly when sliding velocity (SV) increases owing to the development of a rich layer amid the pair's contact area. The addition of MoS_2 particles act as a lubricant and reduce friction between the tribo surfaces. Unreinforced composite in Figure 5(a) shows a maximum wear rate because of direct contact surfaces compared to reinforced composites.

The main effect plot observed in Figure 6(a) and Figure 6(b) for the combined effect of SD and SV revealed a decrease in coefficient of friction (CF). The reduction in friction due to the formation of the MoS_2 layer lay in between the tribo surfaces, act as a lubricant. MoS_2 particles fill the asperities of the worn surface of the pin and stick on the disc, to prevent direct contact between the pin, and the disc is the main cause of reducing the coefficient of friction. Pressure and sliding velocity have an insignificant factor in the coefficient of friction because a thin layer of MoS_2 is almost maintained stably in between the contact surfaces. The wt. % of Al_2O_3 and MoS_2 is the main significant factor that affects the hybrid composite due to their high inclination, as shown in Figure 6(d). The coefficient of friction decreases with the addition of MoS_2 and due to hard phase oxide particles as well form oxide layer between the tribo surfaces. The coefficient of friction is found higher in the base matrix; the high degree of contact between surfaces increases the plastic deformation [8,33]. Similarly, the hard particles (Al_2O_3) is abrasive in nature and lies in between the contact surfaces and surface eroded while pressure increased to cause a high coefficient of friction.

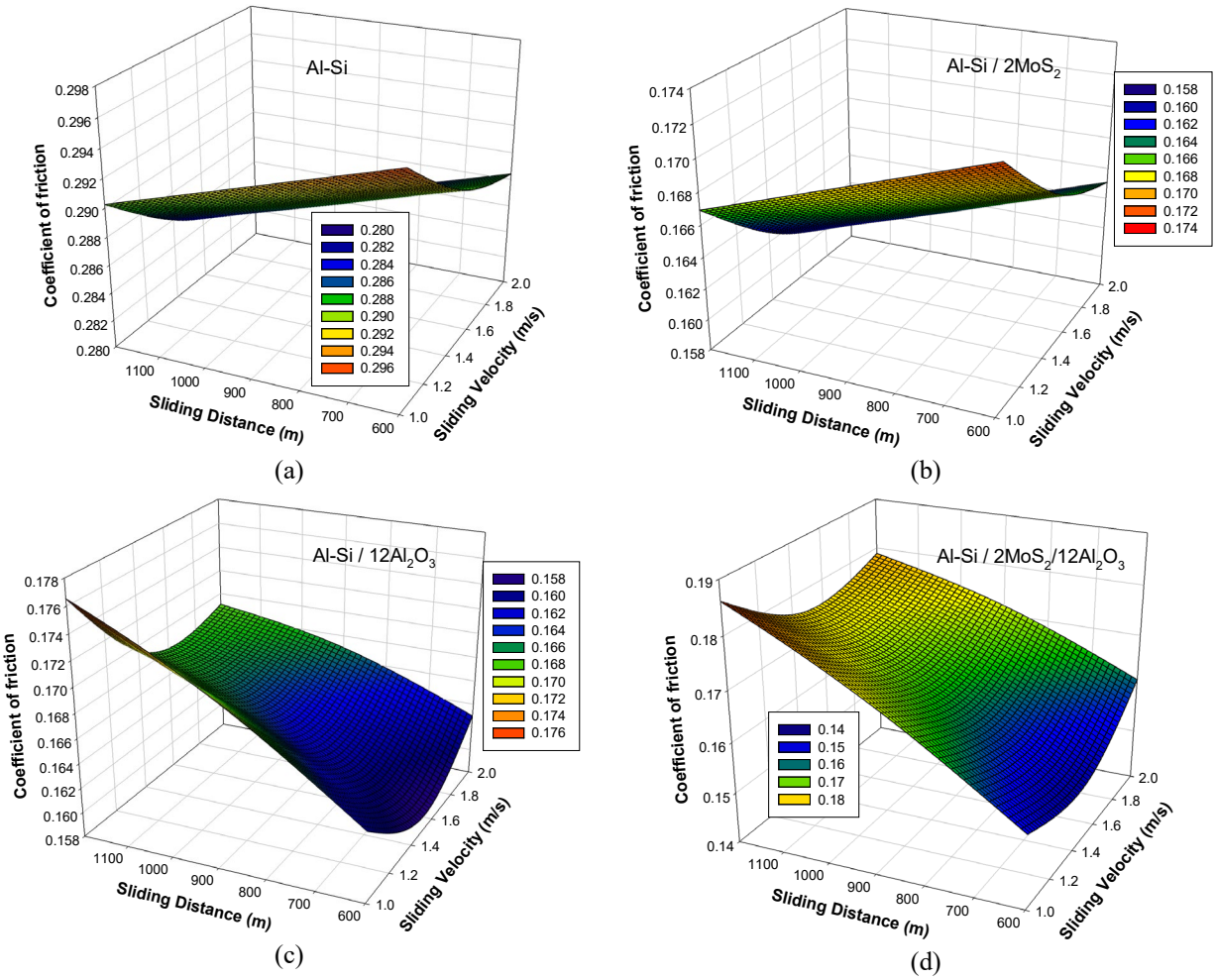

Figure 6. Combined effect of wear rate on composites (a) (a) Al-Si (b) Al-Si/2MoS_2 (c) Al-Si /12Al_2O_3 (d) Al-Si /2MoS_2/12Al_2O_3.

Regression Analysis of Cast Materials

The main purpose of the present study was to investigate optimal operating conditions in order to achieve minimal wear and friction coefficients. The following sections represent individual analysis as well optimal conditions of Al-Si, Al-Si/2MoS_2, Al-Si/12 Al_2O_3, and Al-Si/2MoS_2/12Al_2O_3. The analysis was using Minitab-16 software.

Regression Statistical Analysis for Al-Si Matrix

ANOVA was used to demonstrate the importance of variables and their intervention correlations. According to ANOVA in Table 6, the most important controlling parameter for wear rate is sliding velocity, followed by pressure. Similarly for COF, the highest controlling parameter is pressure followed by sliding velocity. In Table 7, the insignificant parameter is the sliding distance, where found by measuring the p-value. It is also worth noting that R^2 and adjusted R^2 are almost identical, with a confidence interval of 0.084. From Table 7, using the multiple linear regression method, the wear-rate statistical governing equations were established from coefficient of variables as shown in Eq. (1). The positive sign indicates a synergistic impact, whereas the negative signal indicates a contradictory effect.

$$WR\ (Al-Si)\ =\ 2.62103\ -0.66543*\ SV-9.2E-05*SD\ +0.264454*\ P \quad (1)$$

Table 6. ANOVA of Al-Si.

Source	WR				CF			
	SS	DF	Adj MS	% Cont.	SS	DF	Adj MS	% Cont.
SV	27.932	2	13.966	56.92	0.247	2	0.124	17.67
SD	0.961	2	0.48	1.96	0.139	2	0.069	9.91
P	18.397	2	9.198	37.49	1.014	2	0.507	72.44
SV*SD	1.59	4	0.398	3.24	0.001	4	0	0.07
SV*P	0.13	4	0.033	0.27	0.001	4	0	0.07
SD*P	0.061	4	0.015	0.12	0.002	4	0.001	0.14
Error	0.001	8			0.003	8		
Total	49.072	26			1.399	26		

Table 7. Regression analysis of Al-Si.

	WR					CF				
	Coeff.	*Error*	*t Stat*	*P-value*	*p≤0.05*	*Coeff.*	*Error*	*t Stat*	*P-value*	*p≤0.05*
Intercept	2.6E+00	1.0E-01	2.5E+01	3.1E-18	Sig.	2.9E-01	8.1E-04	3.5E+02	1.9E-44	Sig.
SV	-6.7E-01	4.0E-02	-1.7E+01	2.1E-14	Sig.	-7.7E-03	3.1E-04	-2.5E+01	3.8E-18	Sig.
SD	-9.2E-05	6.6E-05	-1.4E+00	1.8E-01	InSig.	-9.7E-06	5.1E-07	-1.9E+01	1.5E-15	Sig.
P	2.6E-01	1.9E-02	1.4E+01	1.7E-12	Sig.	7.7E-03	1.5E-04	5.1E+01	3.2E-25	Sig.
	R^2	Adjusted R^2		Standard error		R^2	Adjusted R^2		Standard error	
	0.953	0.947		0.084		0.994	0.993		0.0007	

Table 7 has no trivial parameters that can be found using p-value estimation. It is also worth noting that R^2 and adjusted R^2 are almost identical, with a standard error of 0.000653. Table 7 uses multiple linear regression method and the statistical formula for CF; developed by means of factors coefficients and Eq. (2) as follows.

$$CF\ (Al-Si)\ =\ 0.2854\ -0.0077*\ SV-9.7E-06*SD\ +0.0077*\ P \quad (2)$$

Figure 7(a) and 7(b) illustrate S/N ratio graphs for various degrees of WR and CF. The optimal parametric option for minimal WR is SV3SD2P1, as with CF is SV3SD3P1, which is 2 m/s of SV, 1200 m of SD, and 2.04 kg-f/cm^2 of P.

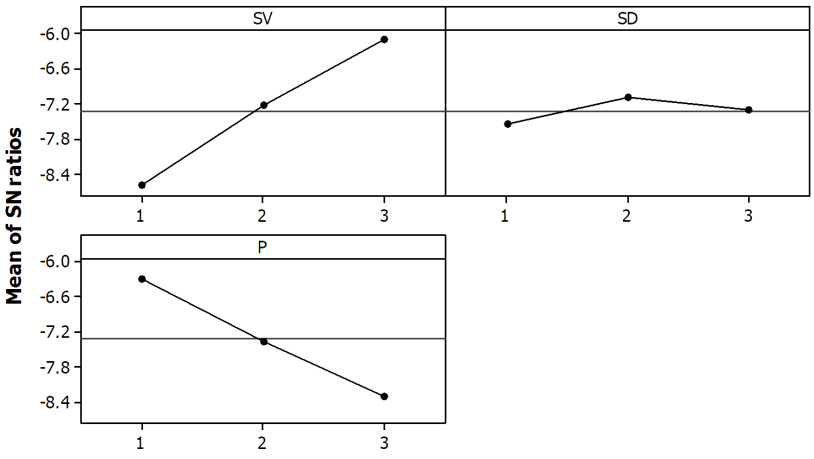

(a)

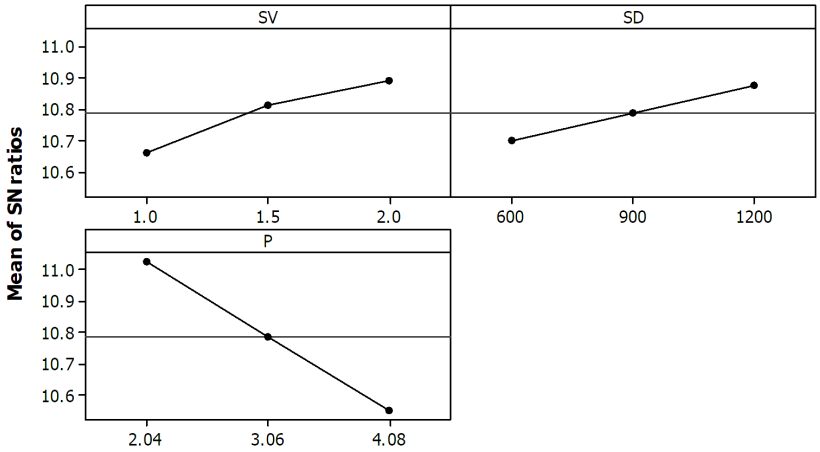

(b)

Figure 7. Covariates effect of Al-Si on (a) WR and (b) CF.

Regression Statistical Analysis for Al-Si / 2MoS$_2$ Composite

As shown in ANOVA from Table 8, pressure is among the most important variables impacting wear rate. Similar to CF, showed that pressure (at 72.43%) is the most important factor, followed by SV (at 17.62%). Table 9 indicates the importance of including all input variables. It should also be noted that R^2 and Adjusted R^2 are essentially equal, with a typical 0.026222 of error. Table 9 uses linear regression analysis and the WR empirical controlling equation is shown in Eq. (3). Table 9 has no trivial parameters that can be found using p-value estimation. It is quite worth remembering that R^2 and adjusted R^2 are almost identical, with a standard error of 0.000653. Table 9 is employing correlation methods, and the empirical mathematical formulation of coefficient of friction formed with factors coefficients is in the following Eq. (4).

$$CF(Al-Si/\ 2MoS2)\ =\ 0.162157\ -\ 0.00767 * SV -\ 9.7E-06 * SD\ +\ 0.007734 * P \quad (4)$$

$$WR\ (Al-Si\ /\ 2MoS2) =\ 1.710982 - 0.30803 * SV + 0.000131 * SD\ + 0.000131 * P \quad (3)$$

Table 8. ANOVA of Al-Si/ 2MoS$_2$.

Source	WR				CF			
	SS	DF	Adj MS	% Cont.	SS	DF	Adj MS	% Cont.
SV	8.083	2	4.042	32.3	0.752	2	0.376	17.62
SD	0.523	2	0.261	2.09	0.423	2	0.212	9.91
P	16.352	2	8.176	65.33	3.092	2	1.546	72.43
SV*SD	0.002	4	0.001	0.01	0	4	0	0
SV*P	0.064	4	0.016	0.25	0.001	4	0	0.03
SD*P	0.004	4	0.001	0.02	0.001	4	0	0.01
Error	0	8			0.001	8		
Total	25.028	26			4.269	26		

Table 9. Regression analysis of Al-Si/ 2MoS$_2$.

	WR					CF				
	Coeff.	*Error*	*t Stat*	*P-value*	*p≤0.05*	*Coeff.*	*Error*	*t Stat*	*P-value*	*p≤0.05*
Intercept	1.7E+00	3.3E-02	5.3E+01	1.8E-25	Sig.	1.6E-01	8.1E-04	2.0E+02	8.5E-39	Sig.
SV	-3.1E-01	1.2E-02	-2.5E+01	3.8E-18	Sig.	-7.7E-03	3.1E-04	-2.5E+01	3.8E-18	Sig.
SD	1.3E-04	2.1E-05	6.4E+00	1.7E-06	Sig.	-9.7E-06	5.1E-07	-1.9E+01	1.5E-15	Sig.
P	2.2E-01	6.1E-03	3.6E+01	1.2E-21	Sig.	7.7E-03	1.5E-04	5.1E+01	3.2E-25	Sig.
	R^2	Adjusted R^2		Standard error		R^2	Adjusted R^2		Standard error	
	0.988	0.987		0.026		0.994	0.993		0.0007	

S/N ratio graphs for specific control factors of WR and CF are shown in Figure 8(a) and Figure 8(b). It was discovered that the optimal parameter configuration for obtaining the lowest wear rate (WR) values is sliding velocity(SV), sliding distance (SD), and pressure (P) at level 3, level 1, and level 1 respectively, represented as SV3SD1P1. Similarly, for the coefficient of friction (CF) the optimal values are sliding velocity (SV) at level 3, sliding distance (SD) at level 3, and pressure (P) at level 1 and denoted as SV3SD3P1.

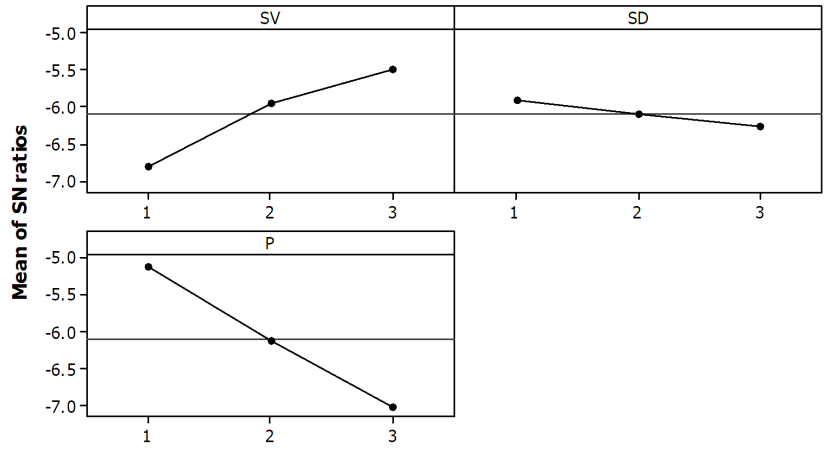

(a)

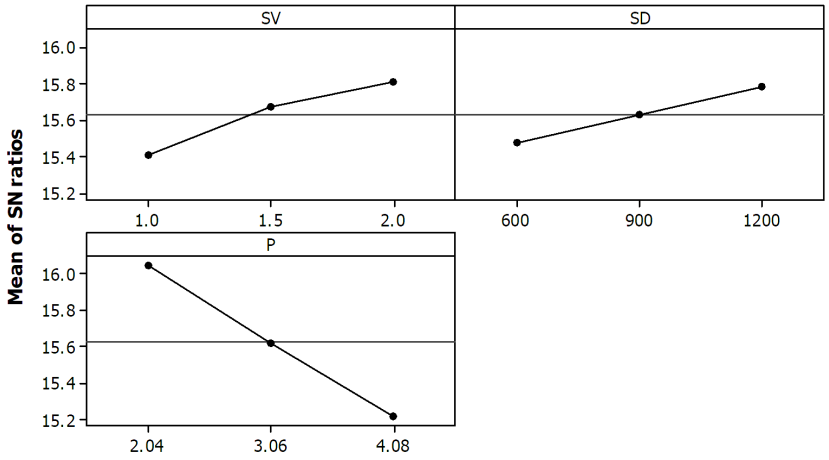

(b)

Figure 8. Covariates effect of Al-Si/2MoS2 on (a) WR and (b) CF.

Regression Statistical Analysis for Al-Si/12Al$_2$O$_3$ Composite

ANOVA in Table 10 illustrated the significant parameter on wear rate is sliding velocity (51.52%) then pressure (33.46%). Likewise, ANOVA of CF shows that pressure (84.27%) is the most influential factor.Table 11 revealed R^2 and Adjusted R^2 are almost similar with 0.12 in error. A regression equation formed with coefficients of wear rate as given in Eq. (5)

$$WR(Al-Si/\ 12Al2O3) = 2.0485 - 0.6038 * SV - 0.00017 * SD + 0.24002 * P \quad (5)$$

Table 11 does not include an irrelevant parameter by calculating p-value. It can also found that R^2 and corrected R^2 are closer and have a 0.002701 defect. The mathematical model equation for a friction coefficient developed using correlation approaches in Table 11 using the coefficients of the variables as in Eq. (6)

$$CF\ (Al-Si/12Al2O3) = 0.117209 - 0.00406 * SV + 1.58E-05 * SD + 0.013611 * P \quad (6)$$

Table 90. ANOVA of Al-Si/ 12Al$_2$O$_3$.

Source	WR				CF			
	SS	DF	Adj MS	% Cont.	SS	DF	Adj MS	% Cont.
SV	44.452	2	22.226	51.52	0.46	2	0.23	4.12
SD	6.319	2	3.16	7.32	1.141	2	0.57	10.21
P	28.869	2	14.434	33.46	9.417	2	4.708	84.27
SV*SD	6.138	4	1.535	7.11	0.089	4	0.022	0.8
SV*P	0.384	4	0.096	0.44	0.031	4	0.008	0.27
SD*P	0.089	4	0.022	0.1	0.036	4	0.009	0.32
Error	0.036	8			0.001	8		
Total	86.287	26			11.174	26		

Table 101. Regression analysis of Al-Si/12Al_2O_3.

	WR					CF				
	Coeff.	Error	t Stat	P-value	p≤0.05	Coefficients	Error	t Stat	P-value	p≤0.05
Intercept	2.0E+00	1.4E-01	1.4E+01	7.9E-13	Sig.	1.2E-01	3.3E-03	3.5E+01	1.9E-21	Sig.
SV	-6.0E-01	5.5E-02	-1.1E+01	1.3E-10	Sig.	-4.1E-03	1.3E-03	-3.2E+00	4.1E-03	Sig.
SD	-1.7E-04	9.2E-05	-1.8E+00	8.4E-02	Sig.	1.6E-05	2.1E-06	7.5E+00	1.4E-07	Sig.
P	2.4E-01	2.7E-02	8.9E+00	6.8E-09	Sig.	1.4E-02	6.2E-04	2.2E+01	7.3E-17	Sig.
	R^2	Adjusted R^2		Standard error		R^2	Adjusted R^2		Standard error	
	0.898	0.885		0.120		0.959	0.954		0.003	

S/N ratio graphs for different factor levels of WR and CF are shown in Figure 9(a) and Figure 9(b). The conclusion is that the optimum variable set for WR is sliding velocity (SV) at level 3, sliding distance (SD) at level 2, and pressure (P) at level 1. Similarly, for coefficient of friction (CF) the optimal values are sliding velocity (SV) at level 2, sliding distance (SD) at level 1, and pressure (P) at level 1, is denoted as SV2SD1P1.

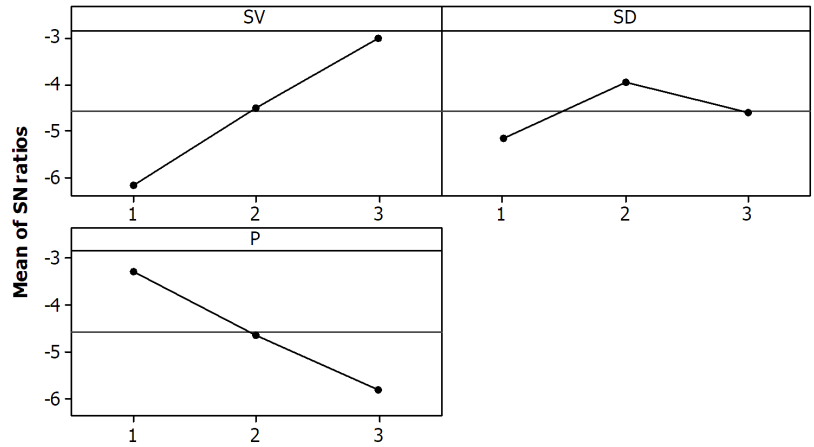

(a)

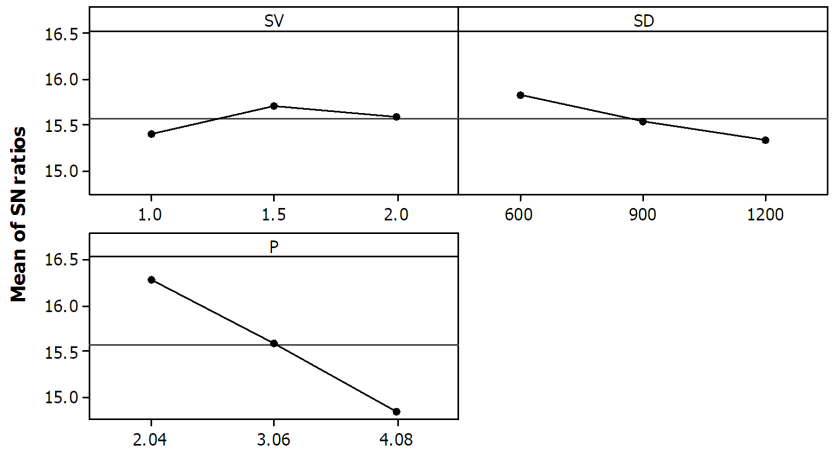

(b)

Figure 9. Covariates effect of Al-Si/12Al_2O_3 on (a) WR and (b) CF.

Regression Statistical Analysis for Al-Si/ 12Al_2O_3 / 2MoS_2 Composite

According to the ANOVA in Table 12, the most controlling parameter for WR and CF is pressure. Table 12 shows that all input variables are important, but Table 13 shows that sliding velocity is negligible. It is indeed worth noting that the expected R^2 agrees reasonably well with the R^2_{adj}, with standard errors of 0.026 and 0.005 for WR and CF, respectively. To use a correlation model, the empirical governing Eq. (7) and (8) for WR and CF are written in the following form:

$$WR\ (Al-Si/\ 12\ Al2O3\ /\ 2MoS2)\ =\ 0.809437-0.30803*\ SV+0.000131*SD\ +0.216403*\ P \quad (7)$$

$$CF\ (Al-Si/\ 12\ Al2O3\ /\ 2MoS2)\ =\ 0.07226-0.00046*\ SV+4.14E-05*SD\ +0.019488*\ P \quad (8)$$

Table 112. ANOVA of Al-Si/12 Al_2O_3/2MoS_2.

Source	WR				CF			
	SS	DF	Adj MS	% Cont.	SS	DF	Adj MS	% Cont.
SV	26.904	2	13.452	31.79	0.800	2	0.400	2.79
SD	1.794	2	0.897	2.12	7.834	2	3.917	27.28
P	55.141	2	27.570	65.16	19.257	2	9.629	67.07
SV*SD	0.024	4	0.006	0.03	0.384	4	0.096	1.34
SV*P	0.706	4	0.177	0.83	0.170	4	0.043	0.59
SD*P	0.050	4	0.013	0.06	0.259	4	0.065	0.90
Error	0.003	8			0.007	8		
Total	84.621	26			28.712	26		

Table 13. Regression analysis of Al-Si/12 Al_2O_3/2MoS_2.

	WR					CF				
	Coeff.	Error	t Stat	P-value	p≤0.05	Coefficients	Error	t Stat	P-value	p≤0.05
Intercept	8.1E-01	3.3E-02	2.5E+01	3.9E-18	Sig.	7.2E-02	6.1E-03	1.2E+01	2.8E-11	Sig.
SV	-3.1E-01	1.2E-02	-2.5E+01	3.8E-18	Sig.	-4.6E-04	2.3E-03	-2.0E-01	8.4E-01	Sig.
SD	1.3E-04	2.1E-05	6.4E+00	1.7E-06	Sig.	4.1E-05	3.9E-06	1.1E+01	2.0E-10	Sig.
P	2.2E-01	6.1E-03	3.6E+01	1.2E-21	Sig.	1.9E-02	1.1E-03	1.7E+01	1.3E-14	Sig.
	R^2	Adjusted R^2		Standard error		R^2	Adjusted R^2		Standard error	
	0.988	0.987		0.026		0.947	0.940		0.005	

Figure 10(a) and 10(b) shows S/N ratio diagram for various parameter levels for WR and CF. It revealed that, the optimal parametric setting is sliding velocity (SV) at level 3, sliding distance (SD) at level 1 and pressure (P) at level 1, (SV3SD1P1), whereas sliding velocity (SV) at level 2, sliding distance (SD) at level 1 and pressure (P) at level 1, is denoted as SV2SD1P1, for WR and CF.

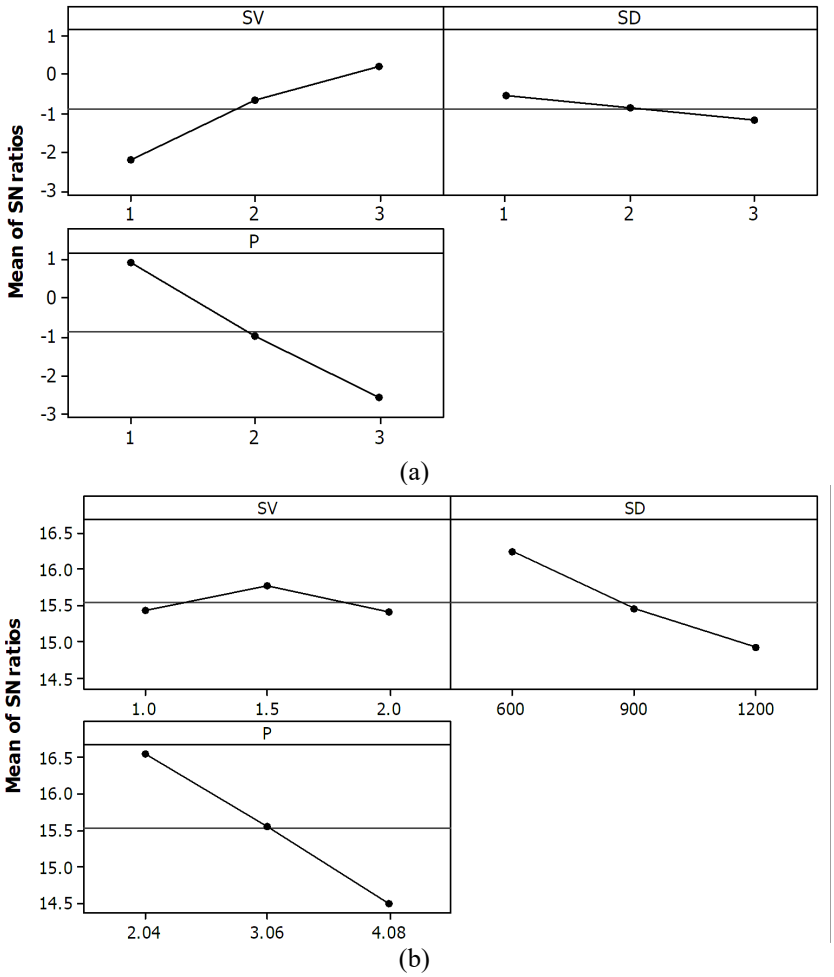

Figure 10. Covariates effect for Al-Si/2MoS_2/12Al_2O_3 on (a) WR and (b) CF.

Linear Regression Analysis of Composites Using Normal Probability of Residuals

The normal probability of residuals plot of wear rate has shown in Figure 11, it revealed that the residuals of composites are scattered randomly about straight lines. It shows that this plot is not consistent, missing phrases, outlines or significant points. From linear regressions, it is clear that while increasing the weight % of MoS_2 and Al_2O_3, wear rate decreased and was clearly defined with slope equations. The composites with MoS_2 having a significant effect on wear resistance and confirmation via R^2 values.

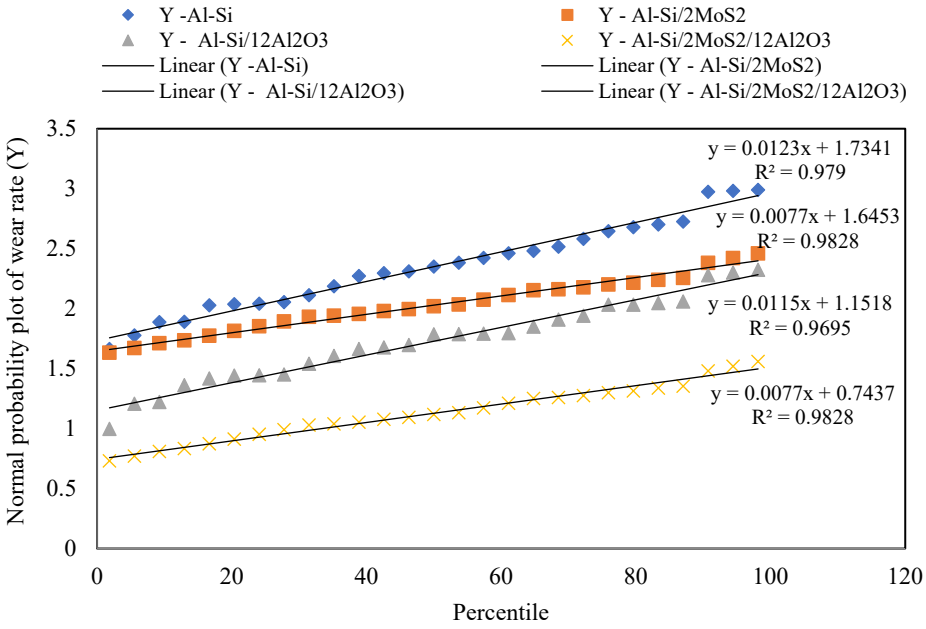

Figure 11. Normal probability of residuals of wear rate.

Similarly, the normal probability distribution of residuals for CF is shown in Figure 12. It cleared that; coefficient of friction for composites exhibited better than base alloy, owing to hard phase reinforced particulates. The linear regression of cast materials exhibited significant responses and having R^2 values greater than 95%.

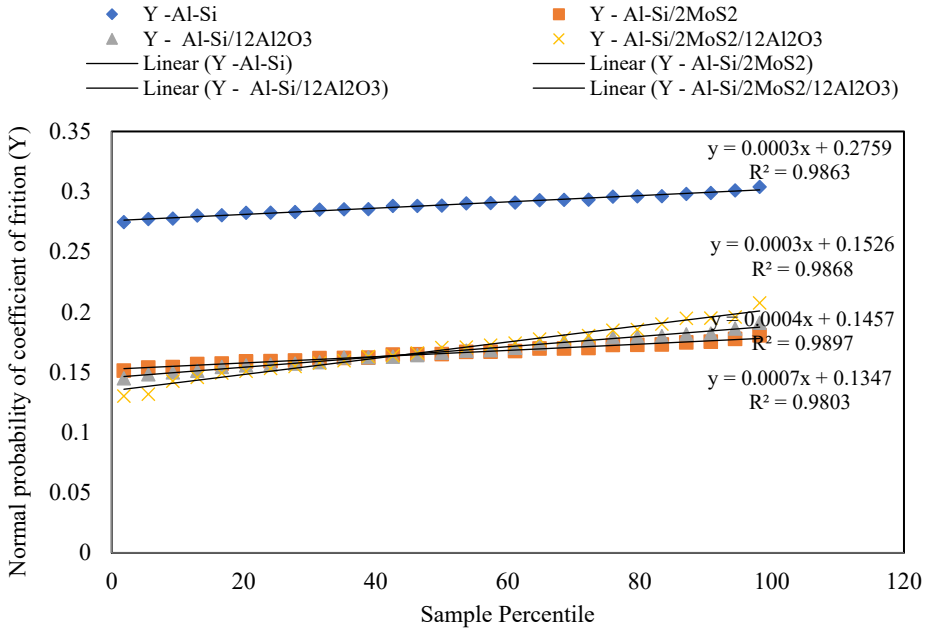

Figure 12. Normal probability distribution of residuals for coefficient of friction.

Surface Morphology Examination

Figure 13 displays the surface morphology of base alloy and cast composites tested at 3.06 kg-f/cm^2(P), 900 m (SD), and 1.5 m/s (SV). The surface of base material in Figure 13(a) simply proves that dislocation density has led to increasing wear rates due to the deep cutting, the existence of large debris on the worn surface. Figure 13(b) shows the worn-out image of the Al-Si /2MoS_2 composite. It can be observed on the surface, uniform pattern of wear, fine residue and burring

at the substrate edge. The MoS_2 establishes an adherent film between the tribo surfaces, which reduces the delamination effect. A sharp layer on the worn surface is described, separating the tribo pair, thus reducing the wear rate [12, 34]. Figure 13(c) depicts the tribo surface of an Al-Si/12Al_2O_3 composite. The pin surface material has been worn even though oxide particles have plugged and broken down. The worn surface indicates that the substance has been degraded and the surface has been abraded. A significant fracture occurs as a result of pair contact, a decrease in hardness, and ductile behaviour [35]. As compared to other composites, the Al-Si alloy exhibits a considerable amount of extreme plastic deformation.

Along with the Al_2O_3 and MoS_2 lubricant reinforcement, the worn surface of a hybrid Al-Si /2MoS_2/12Al_2O_3 composite in Figure 13(d) varies. The composite substrate was flawless, with small grooves and fine debris evident. By analysing the supplied wear tracks, adhesion is visible as adhesion craters inside the wear track, surrounding by parallel grooves indicating abrasion. Adhesion pits vary in shape and size, owing mostly to the material structure in the surface and deeper layers. EDS investigation in Figure 14 reported the presence of elements, which helps to the reduction of friction between tribo surfaces. EDS of hybrid composite referring to SEM image shows adhesion pits and wear tracks confirmed the existence of Fe originating from the steel disc. These results indicate the formation of an oxide layer during dry sliding. Both contact materials respond to atmospheric oxygen. As sliding speed increases, contact temperature rises, promoting oxidation and thickening the oxide layer on both sides. This occurs as a result of direct interaction with oxidized MML.

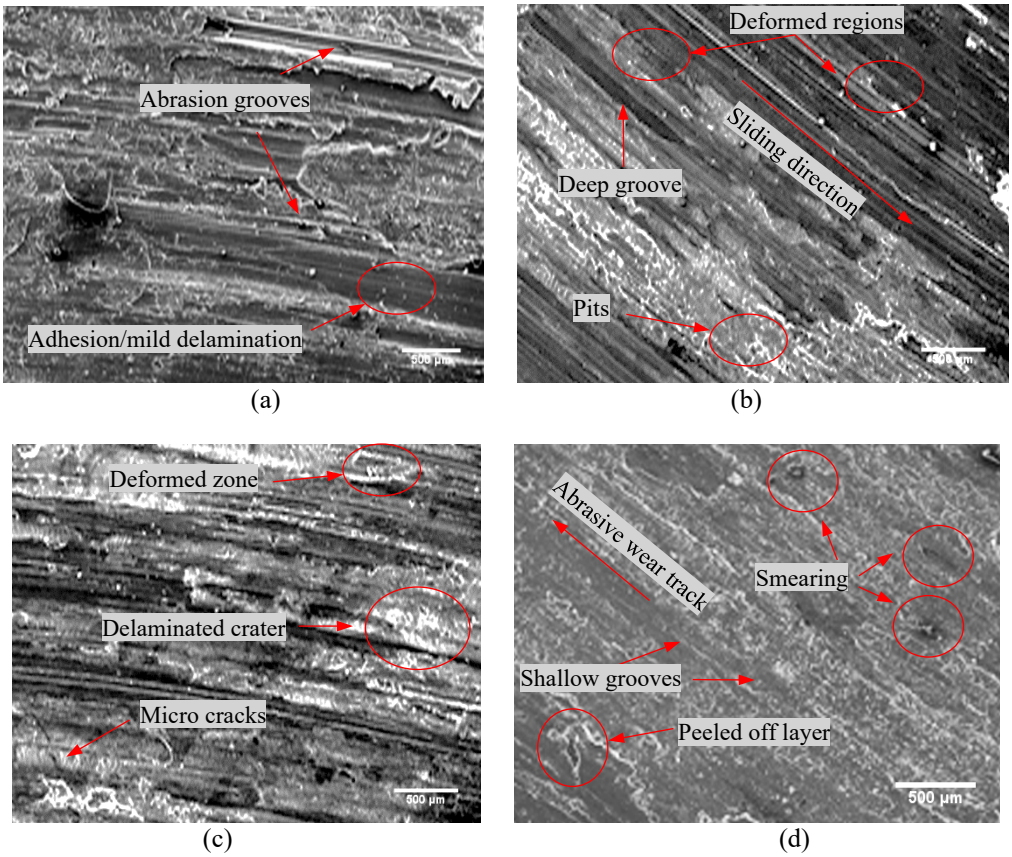

Figure 13. Surface morphological examination of worn-out samples (a) Al-Si (b) Al-Si /2MoS_2 (c) Al-Si /12% Al_2O_{3s} (d) Al-Si /2MoS_2/ 12% Al_2O_3.

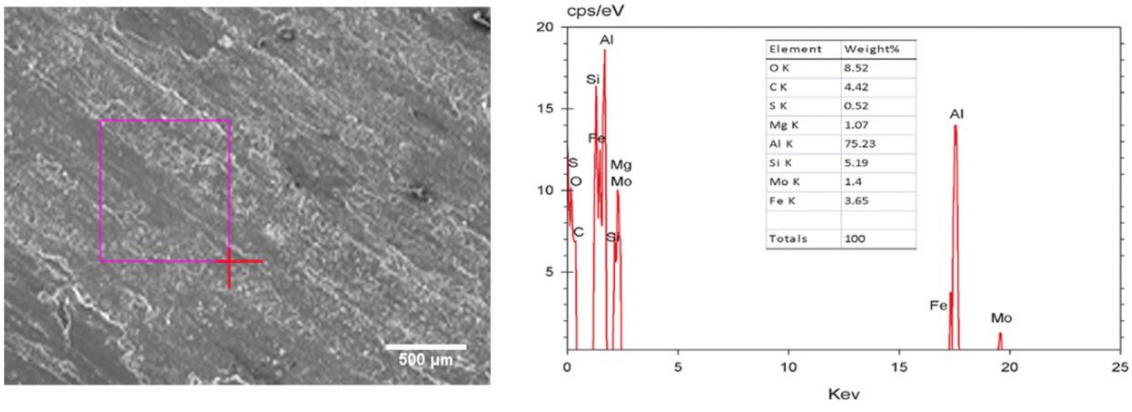

Figure 14. SEM and EDX analysis of worn-out surface of Al-Si/2MoS_2 /12Al_2O_3 composite.

Figure 15 depicts the fluctuation in work hardness with regard to sliding distance. The material gets toughened more quickly after 900 m of sliding distance— work hardening results in increased material hardness, which reduces the rate of wear. The degree of work hardening, on the other hand, increases as that the exerted pressure increases. In this case, the recrystallisation happens due to the Al-excellent alloy's heat conductivity. This reduces hardness in this location, thereby increasing the wear rate [36, 37].

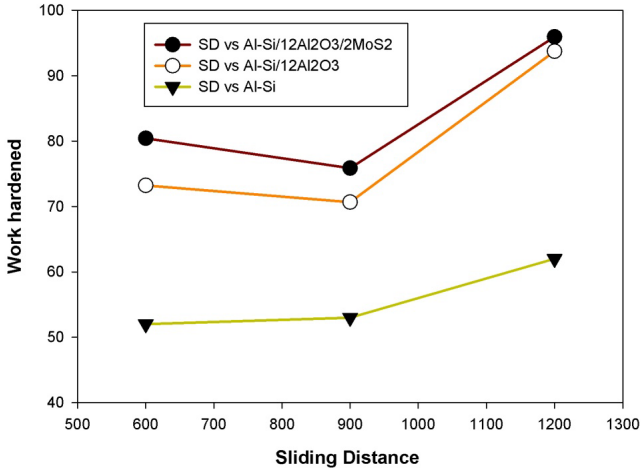

Figure 15 Working effects of composites at specified SV of 1.5 m/s and 3.06 kgf/cm^2 with varied sliding distance.

After wear testing, the worn surfaces of the counterface (steel discs) were also examined with an optical microscope. Figure 16 illustrates the wear track created owing to Al-Si/12Al_2O_3 composite sliding at various applied pressures at counterface. The size of the wear scars is determined by the rate at which the specimens were worn. Figure 16(b) shows abrasion patterns and the narrowest wear scar upon steel disc at low pressure. Abrasion is a predominant mechanism for all pressures due to softening reinforcing material (Al_2O_3 and powder debris) which caused distortion of the wear scars. Figure 16(c) shows the importance of iron oxide debris in the wear track for reducing friction. Deep ploughing marks and delamination as well as excessive plastic deformation with an increase in the applied pressure, are proven to be wear of adhesion [24]. As illustrated in Figure 16(d), deep grooves were detected on the worn surface as a result of strong asperities penetrating the material. The MML creation rate on the tribal surface is quite low, which shows that the oxide layer removal rate is severely reduced in comparison with its production. This could be due to the matrix becoming softer as a result of higher warmth caused by friction. This produces the material's insufficient hardness and strength that worsens the composite wear rate. The MML presence of Al-Si/12Al_2O_3 in the longitudinal area is illustrated in Figure 17. As a result of cracks propagating along the interface between the MML and the pin contact surface, this layer was not completely bonded to the composites. Under the MML, a shattered Al_2O_3 may be seen. Figure 17 show that the MML has an average thickness of 0.812 m.

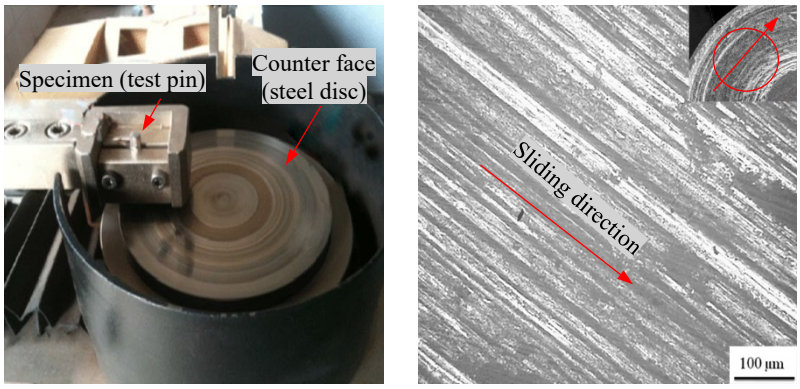

(a) (b)

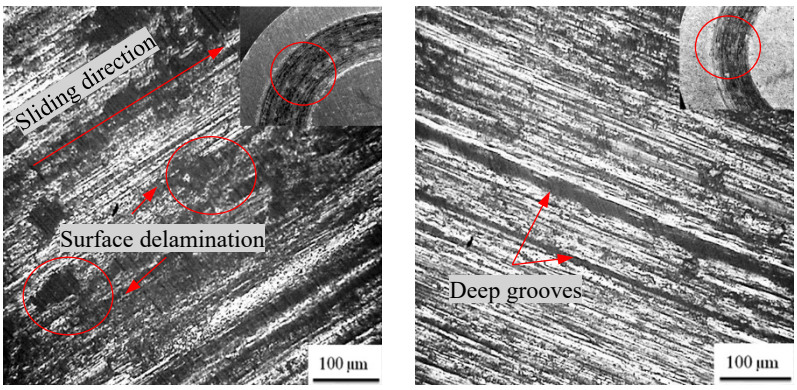

(c) (d)

Figure 16. (a) Metallographic image of specimen mount on steel disc (counter face), and wear track for Al-Si/12Al_2O_3 material at applied pressures of (b) 2.04 kgf/cm^2 (c) 3.06 kgf/cm^2 and (d) 4.08 kgf/cm^2 with a constant SV of 1.5 m/s and SD of 900 m.

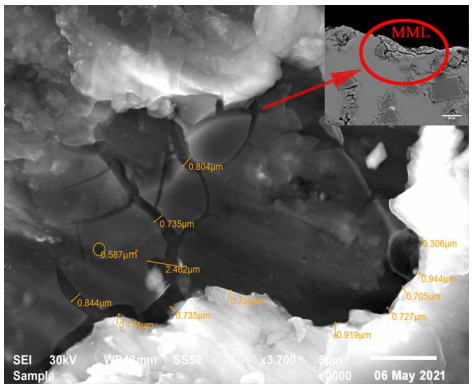

Figure 17. Mechanically mixed layer in longitudinal section of Al-Si/12Al_2O_3 composite.

CONCLUSION

The aim of this study is to develop Al-Si/2MoS_2, Al-Si/12Al_2O_3 and Al-Si/2MoS_2/12Al_2O_3 composites successfully via liquid metallurgical route and also determined optimal tribological performance using Taguchi method. The following are the findings from the survey.

i. As the weight fractions of MoS_2 and Al_2O_3 grew, the density of composites increased. As compared to Al-Si alloy, the density of Al-Si/2MoS_2, Al-Si/12Al_2O_3, and hybrid composites (Al-Si/2MoS_2/12Al_2O_3) raised about 1.15%, 1.84 %, and 2.18%, due to higher density of MoS_2 and Al_2O_3
ii. Al-Si/12Al_2O_3 composite exhibited better tensile strength as compared to hybrid (Al-Si/2MoS_2/12Al_2O_3) composite and strength has enhanced by 11.08% and 2.38% respectively compared to Al-Si matrix, this happens due to MoS_2 in a soft form and has lamellar structure.
iii. Sliding velocity (56.92 %) has the greatest influence on Al-Si of wear rate (WR), while pressure (72.44 %) has the major effect on CF.
iv. The best setting for Al-Si for wear rate is SV3SD2P1, and COF is SV3SD3P1. Pressure (72.43 %) has the strongest impact on Al-Si/2MoS_2 of wear rate (WR), while sliding velocity (51.52 %) has the major effect on the coefficient of friction (CF).
v. The optimum condition of Al-Si/2MoS_2 composite for wear rate (WR) is SV3SD1P1.
vi. Sliding velocity (51.52 %) has the greatest effect on Al-Si/12Al2O3 wear rate, while pressure (84.27 %) has the greatest effect on CF. The best parametric option for Al-Si/12Al_2O_3 composite on WR is SV3SD2P1, while for CF is SV2SD1P1.
vii. The most favourable condition of wear rate for Al-Si/12Al_2O_3/2MoS_2 composite is SV3SD1P1 and for COF is SV2SD1P1.
viii. Taguchi technique is useful in evaluating the tribological responses from the regression equation.
ix. The worn-out surfaces of pin and counter faces were used to study composite wear behaviour.

ACKNOWLEDGEMENT

The author wishes to express his gratitude to Dr Hota Ravisankar (Professor, Department of Mechanical Engineering, GITAM University, Vizag and Andhra Pradesh) for his unwavering support and mentorship throughout my professional career. But I learned devastating news from Covid-19 on May 4, 2021, about his premature demise. In my mind, a genius fell to the ground, putting his family and myself in great peril. I'll never forget your words about advancing my career

and assisting others in a decent manner. You are one of the institute's best teachers, researchers, and all-around nice people. Your guidance, mentorship, and encouragement made me a better person. I will never forget it. I am also indebted to the editorial board of the International Journal of Automotive and Mechanical Engineering (IJAME) for providing me with the opportunity to express my gratitude to my professor.

REFERENCES

[1] A. Salam *et al.*, "Fabrication and tribological behavior of self-lubricating composite impregnated with synthesized inorganic hollow fullerene-like MoS2," *Compos. B. Eng.*, vol. 200, pp. 108284 , 2020, doi: 10.1016/j.compositesb.2020.108284.

[2] S.S. Raju, G.B. Murali, and P.K. Patnaik, "Ranking of Al-CSA composite by MCDM approach using AHP–TOPSIS and MOORA methods," *J. Reinf. Plast. Compos.*, vol. 39, no. 19–20, pp. 721–732, 2020, doi: 10.1177/0731684420924833.

[3] P. Naresh, S.A. Hussain, and B. D. Prasad, "Analysis of dry sliding wear behaviour of AA-7068 / TiC MMCs," *Int. J. Mater. Eng. Innov.*, vol. 11, no. 1, pp. 1–19, 2020, doi: 10.1504/IJMATEI.2020.104788.

[4] N. Radhika, R. Subramanian, and S. V. Prasat, "Tribological behaviour of aluminium / alumina / graphite hybrid metal matrix composite using Taguchi's techniques," *J Miner Mater Char Eng.*, vol. 10, no. 5, pp. 427–443, 2011, doi: 10.4236/JMMCE.2011.105032.

[5] P. Paranthaman, R. R. Babu, and R. Mahesh, "Multi-objective optimization on tribological behaviour of hybrid Al MMC by grey relation analysis," *J. Crit. Rev.*, vol. 7, no. 9, pp. 200–202, 2020, doi: 10.31838/jcr.07.09.42.

[6] L. R. Kumar *et al.*, "Tribological behaviour of AA2219 / MOS 2 metal matrix composites under lubrication," *AIP Conf Proc.*, vol. 2207, no. 1, February, 2020,doi: 10.1063/5.0000042.

[7] N. Radhika *et al.*, "Dry sliding wear behaviour of aluminium / alumina / graphite hybrid metal matrix composites," *Ind. Lubr. Tribol.*, 2012, vol. 64, no. 6, pp. 359–366, doi: 10.1108/00368791211262499.

[8] B.M. Chen, *et al.*, "Effects of MoS2 on tribological properties and mechanically mixed layer of al matrix composites," *Mater. Sci. Forum*, vol. 896 (MSF), p. 83–96, 2017,doi: 10.4028/www.scientific.net/MSF.896.83.

[9] A.J. Haltner, "An evaluation of the role of vapor lubrication mechanisms in MoS2," *Wear*, vol. 7, no. 5, pp. 102–117, 1964, doi: 10.1016 / 0043-1648 (64) 90179-6.

[10] C.P. Koshy, P.K. Rajendrakumar, and M.V., Thottackkad, "Evaluation of the tribological and thermo-physical properties of coconut oil added with MoS2 nanoparticles at elevated temperatures," *Wear*, vol. 330–331, pp. 288–308, 2015, doi: 10.1016/j.wear.2014.12.044.

[11] K.P. Furlan, J.D.B. de Mello, and A.N. Klein, "Self-lubricating composites containing MoS2: A review," *Tribol. Int.,* vol. 120, pp. 280–298, 2018, doi: 10.1016/j.triboint.2017.12.033.

[12] R.K. Upadhyay and A. Kumar, "Epoxy-graphene-MoS2 composites with improved tribological behavior under dry sliding contact," *Tribol. Int.*, vol. 130, June, pp. 106–118, 2019, doi: 10.1016/j.triboint.2018.09.016.

[13] H. Singh, P. Singh, and H. Bhowmick, "Influence of MoS2, H3BO3, and MWCNT additives on the dry and lubricated sliding tribology of AMMC-steel contacts," *J. Tribol.*, vol. 140, no. 4, pp. 1–11, 2018,doi: 10.1115/1.4038957.

[14] G. Srinu and P. Vamsi Krishna, "Performance evaluation of CNT/MoS2 hybrid nanofluid in machining for surface roughness," *Int. J. Automot. Mech. Eng.*, vol. 16, no. 4, pp. 7413–7429, 2019,doi: 10.15282/ijame.16.4.2019.15.0549.

[15] K. Kanthavel, K.R. Sumesh, and P. Saravanakumar, "Study of tribological properties on Al/Al2O3/MoS2 hybrid composite processed by powder metallurgy," *Alex. Eng. J.*, vol. 55, no. 1, pp. 13–17, 2016, doi: 10.1016/j.aej.2016.01.024.

[16] A. Moharami, "High-temperature tribological properties of friction stir processed Al-30Mg2Si composite," *Mater.,* vol. 37, no. 5, pp. 351–356, 2020, doi: 10.1080/09603409.2020.1785792.

[17] A. Moharami *et al.*"Role of Mg2Si particles on mechanical, wear, and corrosion behaviors of friction stir welding of AA6061-T6 and Al-Mg2Si composite," *J. Compos. Mater.*, vol. 54, no. 26, pp. 4035–4057, 2020, doi: 10.1177/0021998320925528.

[18] A. Moharrami *et al.*, "Enhancing the mechanical and tribological properties of Mg2Si-rich aluminum alloys by multi-pass friction stir processing," *Mater. Chem. Phys.*, vol. 250, pp. 123066 (15 pages), 2020, doi: 10.1016/j.matchemphys. 2020.123066.

[19] KS. Vinoth, R. Subramanian, S. Dharmalingam, and B. Anandavel, "Mechanical and tribological characteristics of stir-cast Al-Si10Mg and self-lubricating Al-Si10Mg/MoS 2 composites," *Mater. Tehnol.*, vol. 46, no. 5, pp. 497–501, 2012.

[20] H. Patle *et al.*, "Hardness and sliding wear characteristics of AA7075-T6 surface composites reinforced with B4C and MoS2 particles," *Mater. Res. Express*, vol. 6, no. 8, pp. 086589, 2019,doi: 10.1088/2053-1591/ab1ff4.

[21] N.G. Siddesh Kumar, R. Suresh, and G.S. Shiva Shankar, "High temperature wear behavior of Al2219/n-B4C/MoS2 hybrid metal matrix composites," *Compos. Commun.*, vol. 19, March, pp. 61–73, 2020, doi: 10.1016/j.coco.2020.02.011.

[22] D. Jeyasimman *et al.*, "The effects of various reinforcements on dry sliding wear behaviour of AA 6061 nanocomposites," *Mater. Des.*, vol. 64, pp. 783–793, 2014,doi: 10.1016/j.matdes.2014.08.039.

[23] A. Moharami, "Improving the dry sliding-wear resistance of as-cast Cu-10Sn-1P alloy through accumulative back extrusion (ABE) process," *J. Mater. Res. Technol.,* vol. 9, no. 5, pp. 10091–10096, 2020,doi: 10.1016/j.jmrt.2020.07.022.

[24] R. S.S Raju and B.V. Siva, "Fabrication and tribological studies of Al-CSA composite using RSM," *Int. J. Mater. Eng. Innov.*, vol. 12, no. 2, pp. 83–102, 2021, doi: 10.1504/IJMATEI.2021.115596.

[25] S.R Rallabandi and G. Srinivasa Rao, "Assessment of tribological performance of al-coconut shell ash particulate—MMCs using Grey-fuzzy approach," *J. Inst. Eng. (India): C*, vol. 100, no. 1, pp. 13–22, 2019,doi: 10.1007/s40032-017-0388-4.

[26] P. Booneshwaran *et al.*, "Reduction of casting defects and quality improvement by using Taguchi technique," *Int. J. Mech. Eng. Technol.*, vol. 9, no. 11, pp. 1327–1338, 2018.

[27] T. Bement, "Taguchi techniques for quality engineering," *Technometrics*, vol. 31, no. 2, p. 253–255, 1989,doi: 10.1080/00401706.1989.10488519.

[28] M.I. Pech-Canul, "Aluminum alloys for Al/SiC composites," in *Recent Trends in Processing and Degradation of Aluminum Alloys,* Ahmad Z, Eds. InTech, 2011, pp. 299–314.

[29] R Jojith and N. Radhika, "Mechanical and tribological properties of LM13/TiO2/MoS2 hybrid metal matrix composite synthesized by stir casting," *Part. Sci. Technol.*, vol. 37, no. 5, pp. 566–578, 2019, doi: 10.1080/02726351.2017.1407381.

[30] G. Moona *et al.*"Aluminium metal matrix composites: A retrospective investigation," *Indian J. Pure Appl. Phys.*, vol. 56, no. 2, pp. 164–175, 2018,.

[31] T. Miyajima and Y. Iwai, "Effects of reinforcements on sliding wear behavior of aluminum matrix composites," *Wear*, vol. 255, no. 1-6, pp. 606–616, 2003, doi: 10.1016/S0043-1648(03)00066-8.

[32] Y. Sahin, "Wear behaviour of aluminium alloy and its composites reinforced by SiC particles using statistical analysis," *Mater. Des.*, vol. 24, no. 2, pp. 95–103, 2003, doi: 10.1016/S0261-3069(02)00143-7.

[33] G. Pitchayyapillai *et al.*"Al6061 hybrid metal matrix composite reinforced with alumina and molybdenum disulphide," *Adv. Mater. Sci. Eng.*, vol. 2016, article ID: 6127624, pp. 1–9, 2016, doi: 10.1155/2016/6127624.

[34] Y.C. Lin *et al.*, "Wear and friction characteristics of surface-modified aluminium alloys," *Int. J. Surf. Sci. Eng.*, vol. 9, no. 2/3, pp. 109–123, 2015, doi: 10.1504/IJSURFSE.2015.068236.

[35] A. Moharrami *et al.*, "Effect of tool pin profile on the microstructure and tribological properties of friction stir processed Al-20 wt% Mg2Si composite," *J. Tribol.*, vol. 141, no. 12, 122202 (10 pages) 2019,doi: 10.1115/1.4044672.

[36] R.S. Sankara Raju *et al.*, "Tribological behaviour of Al-1100-coconut shell ash (CSA) composite at elevated temperature," *Tribol. Int.*, vol. 129, pp. 55–66, 2019,doi: 10.1016/j.triboint.2018.08.011.

[37] S. Fu *et al.*, "Effects of particle size, particle / matrix interface adhesion and particle loading on mechanical properties of particulate–polymer composites," *Compos. B. Eng.*, vol. 39, no. 6, p. 933–961, 2008, doi: 10.1016/j.compositesb.2008.01.002.